Modulating self-assembly of a nanotape-forming peptide amphiphile with an oppositely charged surfactant

Article

Accepted Version

Modulating Self-Assembly of a Nanotape-Forming Peptide Amphiphile with an Oppositely Charged Surfactant

Valeria Castelletto, Ian W. Hamley*
School of Chemistry, Food and Pharmacy, University of Reading, Reading RG6 6AD, UK

Jozef Adamcik, Raffaele Mezzenga*
ETH Zurich, Food & Soft Materials Science, Institute of Food, Nutrition & Health, Schmelzbergstrasse 9, LFO, E23, 8092 Zürich, Switzerland

Jeremie Gummel
European Synchrotron Radiation Facility, BP 220, 38043 Grenoble Cedex 9, France

For Soft Matter. Revised 20/10/11.

* Authors for correspondence.
I.W.Hamley@reading.ac.uk, tel. 44 118 378 6341 fax 44 118 378 8450;
Raffaele.mezzenga@agrl.ethz.ch.

Abstract

A peptide amphiphile (PA) C_{16}-KTTKS containing a pentapeptide headgroup based on a sequence from procollagen I attached to a hexadecyl lipid chain, self-assembles into extended nanotapes in aqueous solution. The tapes are based on bilayer structures, with a 5.2 nm spacing. Here, we investigate the effect of addition of the oppositely charged anionic surfactant sodium dodecyl sulfate (SDS) via AFM, electron microscopic methods, small-angle X-ray scattering and X-ray diffraction among other methods. We show that addition of SDS leads to a transition from tapes to fibrils, via intermediate states that include twisted ribbons. Addition of SDS is also shown to enhance the development of remarkable lateral "stripes" on the nanostructures, which have a 4 nm periodicity. This is ascribed to counterion condensation. The transition in the nanostructure leads to changes in macroscopic properties, in particular a transition from sol to gel is noted on increasing SDS (with a further re-entrant transition to sol on further increase of SDS concentration). Formation of a gel may be useful in applications of this PA in skincare applications and we show that this can be controlled via development of a network of fine stranded fibrils.

Introduction

A peptide amphiphile (PA) is a hybrid molecule that combines the properties of a lipid (tendency for membrane formation, enhanced bioavailability) with that of a peptide (defined secondary structures, wide biofunctionalisation). PA-based materials are attracting immense attention due to a diverse range of demonstrated potential applications in regenerative medicine.[1-4] Studies on the self-assembly of peptide amphiphiles[5-9] reveal that the most common motif is that of nanofibrils, comprising a lipid core decorated with a peptide corona. Nanotapes have also been identified.[10, 11] Stupp and coworkers also noted stripes (grooves) in their tape-forming PA system, C_{16}-OVEVE, upon increase in pH resulted from electrostatic repulsion among glutamate groups at higher pH.[10] Their model suggests a simple lateral expansion of interdigitated PA molecules. Despite this recent work, little is known about how the driving forces for self-assembly can be modulated via, for instance formation of electrostatic complexes with charged surfactants.

We recently investigated the self-assembly of PA C_{16}-KTTKS in aqueous solution. [11] This PA contains a matrikine (extracellular matrix-derived peptides) pentapeptide fragment from type I collagen.[12] Formulations containing this PA are available commercially as Matrixyl™. Tape-like nanostructures were observed, with a broad distribution of widths. The highly extended tape-like structures aggregate into fibrillar bundles which are large enough to be imaged by optical microscopy. The nanostructure of the tapes was probed by cryogenic-transmission electron microscopy (cryo-TEM) and small-angle X-ray scattering (SAXS). SAXS on an aligned sample enabled a model of bilayers running parallel to the tape surfaces to be put forward. Here, we present preliminary results from a very extensive investigation on

morphology transitions in PA C_{16}-KTTKS induced by addition of the classical anionic surfactant sodium dodecyl sulfate (SDS). This is investigated in detail through atomic force microscopy (AFM), transmission electron microscopy (TEM) and scanning TEM (STEM) as well as small-angle X-ray scattering (SAXS) and X-ray diffraction (XRD). FTIR spectroscopy is used to investigate features of β-sheet ordering in the amide I' region. A complex interplay of electrostatic, hydrophobic and hydrogen bonding interactions leads to a transition from tapes to fibrils on increasing [SDS]. Electrostatic interactions involving the lysine side chains and the carboxyl terminus of the PA are expected to be important. However, electrostatic interactions are not solely responsible for the self-assembly process as revealed by electrophoretic mobility measurements. In addition, we observe the formation of longitudinal stripes on these aggregates. This is analysed in some detail and a model for the structure is presented. The morphological transitions also lead to changes in rheological properties specifically a sequence of transitions sol – gel – sol on increasing [SDS]. The observation of a gel (at intermediate [SDS] = 0.3 wt%) is an interesting finding with potential in applications of this PA in skincare (current application, at market) or tissue engineering (potential application). The ability to tune macroscopic properties such as rheology through control of self-assembled aggregate structure via addition of SDS is a notable aspect of this research. The gel is formed from a network of extended, fine-stranded fibrils.

The effect of electrostatic interactions on the self-assembly of PAs via multicomponent formulations has already been considered. Stupp and coworkers have examined the formation of nanofibers by electrostatic co-assembly of two PAs with oppositely charged peptide sequences.[13] This group also studied the coassembly of

PAs with oppositely charged, i.e. free N and free C termini, comprising respectively tri-lysine and tri-glutamic acid sequences.[14] They noted that the coassembled PA nanofibrils exhibited enhanced thermal stability compared to the component PAs. Aulisa *et al*. have investigated the self-assembly of several short designer PAs and showed that one that had the ability to inhibit proliferation of pancreatic cancer cells self-assembles into micelles at low concentration.[15] This designer PA was mixed with an anionic surfactant, sodium dodecyl sulphate (SDS), and a concomitant increase in α-helical content was noted. Nonetheless, we are not aware of prior work on the influence of surfactants on the self-assembly of PAs forming β-sheet structures and we discuss this problem for the first time in the following.

Experimental

Materials.

Peptide amphiphile C_{16}-KTTKS, Palmitoyl-Lys-Thr-Thr-Lys-Ser was purchased from CS Bio (Menlo Park, California). Two different batches were used. For the first, the purity was 97.6% by analytical HPLC, MS 802.47 (expected) 802.05 (measured), acetate content was 11% (by HPLC). For the second batch, the purity was 98.61% by analytical HPLC, MS 802.5 (expected) 802.2 (measured), acetate content was 11.61% (by HPLC).

Sodium dodecyl sulfate (SDS, 99% purity) was obtained from Sigma Aldrich.

The peptide was dissolved directly in water (along with varying amounts of SDS) for the experiments reported herein. The measured pH of a 1 wt% solution (the concentration for the majority of the measurements) was pH 4.475.

Scanning Transmission Electron Microscopy (STEM).

STEM imaging and associated quantitative analysis (mass per unit area) were performed at the STEM facility, in the Biology Department at Brookhaven National Laboratory using a custom-built instrument. Further details are provided elsewhere.[16, 17]

Negative Stain Transmission Electron Microscopy (TEM).

TEM experiments were performed using a Philips CM20 transmission electron microscope operated at 80kV while high resolution TEM (HR-TEM) was done using a JEOL JEM-4000 microscope operated at 200 kV. Droplets of the solutions were placed on Cu grids coated with a carbon film (Agar Scientific, UK), stained with uranyl acetate (1 wt %) (Agar Scientific, UK) and dried.

Atomic Force Microscopy (AFM).

A 20 µl of solution (1 wt% of C_{16}-KTTKS with different SDS concentrations) were deposited onto freshly cleaved mica, incubated for 2 min, rinsed with Milli-Q water and dried by air. Tapping mode AFM was carried out on a Nanoscope 8 Multimode Scanning Force Microscope (Veeco). AFM cantilevers (Veeco, USA) for tapping mode in soft tapping conditions were used at a vibrating frequency of 150 kHz. Images were simply flattened using the Nanoscope 8.1 software, and no further image processing was carried out. The height profiles were obtained with same software.

Electrophoretic Mobility

Electrophoretic mobility of C_{16}-KTTKS:SDS mixtures was determined by the Zetasizer Nano ZS dynamic light scattering device (Malvern Instruments,

Worcestershire, UK). Samples were inserted in plastic, folded capillary cells (Malvern Instruments), possessing two metal electrodes at each end of the capillary. Motion of the aggregates was measured by laser light scattering in a pulsed electric field, which is a function of electric field strength, dielectric constant and viscosity of the media, and the ζ-potential of the particle.

Small-Angle X-ray Scattering (SAXS)

Experiments were performed on beamline ID02 at the ESRF, Grenoble, France. Samples were placed in a glass capillary mounted in a brass block for temperature control. Micropumping was used to minimise beam damage, by displacing a drop of the sample by 0.01-0.1 mm for each exposure. The sample-to-detector distance was 1 m, and the x-ray energy was 12.46 keV. The $q = 4\pi\sin\theta/\lambda$ (2θ is the scattering angle and λ is the wavelength) range was calibrated using silver behenate. Data processing (background subtraction, radial averaging) was performed using the software SAXSUtilities.

Fibre X-Ray Diffraction (XRD)

X-ray diffraction was performed on stalks prepared from 1 wt% solutions in water or aqueous SDS solution. The stalks were mounted (vertically) onto the four axis goniometer of a RAXIS IV++ X-ray diffractometer (Rigaku) equipped with a rotating anode generator. The XRD data was collected using a Saturn 992 CCD camera. One-dimensional profiles in the equatorial and meridional reflections (with appropriate re-alignment of images to allow for fibril orientation) were obtained using the software CLEARER[18] which was also used to fit peak positions.

Fourier Transform Infrared (FTIR) Spectroscopy

Spectra were recorded using a Nexus-FTIR spectrometer equipped with a DTGS detector. Solutions were sandwiched in ring spacers between two CaF_2 plate windows (spacer 0.006 mm). All spectra were scanned 128 times over the range of 4000-950 cm^{-1}.

Rheology

Measurements of dynamic shear modulus were performed using a TA instruments AR-2000 controlled stress rheometer. A cone and plate geometry (20mm diameter, 1° angle) was used for all samples. Frequency sweeps were performed in the angular frequency (ω) range 0.1-600 rad/s with the instrument in oscillatory mode at 20 °C and a controlled stress (σ < 0.1 Pa). Temperature ramps, heating at 2 $^oC\ min^{-1}$ or 3 $^oC\ min^{-1}$, were made between 20 and 70 ^oC, fixing the frequency at a 6 rad s^{-1} for the data shown here. Temperature ramps and stress sweeps were performed choosing a controlled oscillatory stress within the linear regime

Results

AFM was also used at first to study the morphology of aggregates in solutions of C_{16}-KTTKS in the absence and presence of SDS at different concentrations. Figure 1 shows unambiguously the presence of multi-layered tapes. By analysis of height profile we obtained the value for the step of the single layer to be 5.3 nm. This periodicity is in excellent agreement with the value found in previous work by SAXS[11] and the further analysis given below. Additionally, smaller steps could be identified of height 2.65 nm. This corresponds to exactly half a layer and indicates

convincingly that bilayers of C_{16}-KTTKS and single layers of C_{16}-KTTKS can be resolved by AFM analysis.

We have then performed similar height profile analysis for C_{16}-KTTKS with different [SDS] (Fig. 2). Without SDS the transversal height profile (red curve, 0% SDS) reaches constant maximum plateau values reflecting the flatness of the tape shapes. The longitudinal height profile (black curve, 0% SDS) is constant, indicating uniform cross-sectional heights. In the presence of 0.2 wt% SDS, the transversal height profile (red curve, 0.2% SDS) becomes a mixture of contributions with both maximum plateau heights and sharp peaks, indicating the coexistence of flat tapes together with cylindrical shapes. This is confirmed by the longitudinal height profile, which exhibit both the constant profile typical of flat tapes (blue curve, 0.2% SDS) and also the zig-zig profile typical of twisted ribbons (black curve, 0.2% SDS).[19-21] At a concentration of 0.3 wt% of SDS mainly twisted structures were observed (black and red curves, 0.3% SDS). This was confirmed by negative stain TEM (SI Fig.1a). At even higher SDS concentration (0.6 wt %), the transversal height profile (red curve) is peaked (e.g. without plateau), but the longitudinal profile is now constant (black curve, 0.6% SDS), which clearly indicates that the twisted structures have disappeared to leave fibrils with a cylindrical-like morphology. The formation of fibrillar structures at high [SDS] is confirmed by negative stain TEM (SI Fig.1b).

At the even higher concentration of SDS (0.9 wt%), stripes with a periodicity about 4.2 nm, typical of SDS periodicity, can clearly be resolved on the surface of the aggregates (Fig. 3) in a high magnification image. Actually, stripes are present at

lower [SDS] also, as discussed shortly, but since the spacing is only 4 nm, they are only revealed on high resolution images.

These data taken together would suggest that SDS drives a transition from mainly tapes to mainly fibrils in the regime [SDS] < 0.6 wt% and further that a longitudinal stripe pattern with a 4 nm spacing develops, being particularly notable at 0.9 wt% SDS.

In view of the recent study illustrating that the pitch and shape of twisted ribbons can be modulated by electrostatic interactions,[22] we also performed electrophoretic mobility studies on the C_{16}-KTTKS/SDS mixtures. Our measurements indicate an electrophoretic mobility of +4.798, -3.656 and -7.555 μm*cm/Vs for 0%, 0.3% and 0.6% SDS, respectively, which reflects the progressive change of linear charge density from positive (C_{16}-KTTKS) to negative (SDS) upon increasing [SDS] concentration. The system with SDS contains a complex set of equilibria between ionic species. In order to understand the influence of charge on the C_{16}-KTTKS PA we calculate the degree of dissociation of the N terminus. SI Fig.2 shows the calculated fraction of species with C termini comprising carboxylate or carboxylic acid. The calculation was performed using the freely-available software HySS, designed to calculate properties associated with solution equilibria.[23] This calculation was performed assuming pKa(Lys1) = pKa(Lys2) = 10.4 and pKa(α-carboxyl) = 3.0.[20] It can be seen that the fraction of charged termini decreases with increasing PA concentration. In the following, we investigate the system at a concentration of 1 wt% C_{16}-KTTKS. Under these conditions, the fraction of carboxylate end groups is calculated to be approximately 0.25. The majority of the PA molecules are then

expected to have a net charge +2, although a fraction (around one quarter) will have net charge +1. Based on this estimation, we would expect that the charge neutrality condition in mixtures with dodecyl sulphate for the majority of the PA molecules will occur at a molar ratio 1.75: 2 of C_{16}-KTTKS: dodecyl sulphate. This translates into a weight ratio of 2.6: 1. In the following, the concentration of C_{16}-KTTKS is maintained at 1 wt% in water. The electroneutrality condition would therefore be expected at approximately 0.38 wt% SDS, based on the calculation. Results of the electrophoretic mobility experiments, however, indicate that neutrality is achieved at concentrations well below 0.3 wt% SDS. which is probably due to the simplified nature of this calculation, in which the equilibria involving SDS and its counterions have been neglected). It may be noted that this value is above the cmc of SDS which is 0.23 wt% SDS at 25 ^{o}C[24-27] increasing to 0.33 wt% at 50 ^{o}C.[24]

The immediate outcome from the electrophoretic mobility analysis is that changes in morphologies in the present case cannot only be interpreted on the basis of electrostatic interactions. Comparable charge densities, probed via electrophoretic mobilities, but with opposite signs, result on completely different morphologies, i.e. flat tapes for 0 wt% SDS but twisted ribbons for 0.3 wt% SDS. This complex behavior, which is not observed in ribbons and twisted ribbon-like structures when electrostatic interactions are solely tuned by ionic strength,[22] is probably the result of the multitude of factors relevant and specific to the present case, where the multi-component formulation, the possible heterogeneities, the variable charge density, counter-ion condensation, chirality, hydrogen bonding, hydrophobic interactions and packing frustration due to the alkyl chain length mismatch between C_{16}-KTTKS and SDS, all play a very complex and intricate role.

In order to further elucidate the structure of tapes of C_{16}-KTTKS in the absence and presence of SDS, electron microscopy was also used. In particular, this technique was used to confirm the formation of stripes on tape-like aggregates even at low [SDS]. Fig.4 shows images obtained by scanning transmission electron microscopy (STEM) and negative stain TEM. SI Fig.3 shows additional images. STEM was used to for quantitative analysis of mass per unit area. Fig.4a shows a representative STEM image of a bilayer tape. The mass per unit area was found to be 58 Da/Å^2 for bilayer tapes and half this value for very rare monolayer tapes (an example is shown in SI Fig. 1b). These values indicate that the cross-sectional area per PA molecule is 27.6 Å^2.

TEM shows lateral stripes within a proportion of tapes formed by Matrixyl at 1 wt% and increasingly upon adding SDS (up to 0.9% SDS at which concentration the tapes are disrupted). A representative TEM image is shown in Fig.4b. Fourier transformation was used to determine the stripe spacing 4 nm. In contrast, stripes were not seen clearly by STEM, which was used to examine the thinnest tapes of the PA (one bilayer or less thick).

Real space imaging was complemented by small-angle x-ray scattering on solutions, and x-ray diffraction from dried stalks. SAXS profiles for 1 wt% solutions of C_{16}-KTTKS with varying concentration of SDS in the range 0 – 0.9 wt% at 25 ^{o}C are shown in Fig.5a. This data reveals a wealth of features. For C_{16}-KTTKS without added SDS the profiles show the presence of a peak at q = (1.20 ± 0.01) nm^{-1} with

second and third order reflections, consistent with a layered structure with (5.24 ± 0.05) nm spacing, which corresponds to the period of C_{16}-KTTKS bilayers.[11] Upon addition of 0.1 wt% SDS, a small broad peak appears at q = 1.77 nm^{-1}. This evolves on increasing [SDS] into a peak at q = 1.56 nm^{-1}, corresponding to a period 4.0 nm. This agrees with the spacing of stripes observed by TEM and AFM. A further feature that develops at higher SDS concentration is associated with the formation of a broad maximum at q = 0.5-0.6 nm^{-1}, which we ascribe to the structure factor of self-assembled of SDS micelles (above the cmc, which is 0.23 wt% at 25 ^{o}C[24, 27]) for which a broad structure factor maximum around q = 0.7 nm^{-1} has been observed. [28, 29] Importantly, the broad form factor maximum for SDS micelles (radius approximately 2 nm[28, 30]) occurs at a significantly larger q value than the peak positions associated with the stripe and bilayer spacings, so there is no significant interference from SDS micelle features at high [SDS].

Fig.5b shows temperature-dependent SAXS data for 1 wt% C_{16}-KTTKS on its own and for 1 wt% solutions with SDS at four selected concentrations. There is no temperature dependence in the range 25 – 55 ^{o}C studied for C_{16}-KTTKS on its own, however for the sample with 0.3 wt% SDS a transition is observed on heating from a profile that contains peaks corresponding to both 5.2 nm and 4.0 nm spacings, to one with just the 5.2 nm bilayer peak. A similar trend is observed at higher SDS concentrations, with the difference that the 4.0 nm peak at 25 ^{o}C is intense (more intense than the 5.2 nm spacing for 0.6% SDS) and does not disappear at high temperature for the 0.6 wt% SDS and 0.4% SDS samples, but rather decreases to a lower intensity than that of the 5.2 nm peak. These observations point to a balance between electrostatic and thermal effects. Specifically, these observations are

consistent with the general observation that increasing temperature favours miscibility of the co-surfactant. Further quantitative analysis is beyond the scope of this paper.

SAXS was also performed on samples aligned by shear flow, to examine orientation effects. Fig.6a shows a representative pattern. This reveals that under flow, tapes align along the flow direction and Bragg peaks corresponding to both 5.2 nm and 4.0 nm spacings (consistent with the 1D profiles shown in Fig.5) are observed perpendicular to the flow direction. This indicates that both of these periodicities are perpendicular to the tape long axis.

Fibre X-ray diffraction was used to investigate ordering at the level of the β-sheet structure, in addition to the layer and stripe spacings. Stalks were prepared by drying solutions of 1 wt% C_{16}-KTTKS with and without SDS. All patterns presented high quality cross-β like patterns showing β-sheet ordering of the PA. The corresponding diffraction patterns are shown in Fig.6b, and the spacings are listed in Table 1. These results firstly confirm findings from SAXS discussed above. Up to and including 0.3 wt% SDS, spacings corresponding to the 5.2 nm bilayer structure are observed - specifically, the second and fourth order reflections along with the third, in some cases. This confirms lamellar ordering of the 5.2 nm bilayers. At higher [SDS], these peaks are weaker, with a 4 nm stripe spacing and associated higher order reflections predominating. Another interesting feature from the fibre XRD data is that the spacing of the backbones in the PA (β-strand spacing) changes upon addition of SDS, above 0.3 wt% SDS, which is also the concentration at which the 4 nm stripe spacing

starts to appear. Above [SDS] = 0.3 wt%, we believe additional electrostatic repulsion between side groups leads to an expansion of the β-sheet spacing distance from 1.15 nm to 1.2 – 1.3 nm (Table 1) along with a concomitant small reduction in the spacing of strands within a β-sheet. The strand spacing for 1 wt% C_{16}-KTTKS with no added SDS is in agreement with the calculated mass density value obtained from STEM (4.8 × 5.75 Å area per PA molecule), as discussed above.

FTIR spectroscopy was performed to investigate the presence of β-sheet structures as a function of [SDS] and temperature. Fig.7a shows FTIR spectra in the amide I' region at 25 ^{o}C for different SDS concentrations. The strong peak at 1608 cm^{-1} is consistent with β-sheet secondary structure. Since there is no additional peak in the range 1680 – 1690 cm^{-1}, the structure can be assigned as parallel β-sheets. This is consistent with the constraint on the peptides imposed by the bilayer structure of the PA molecules. A further peak at 1651 cm^{-1} can be assigned to disordered structure, this is significantly less intense than the β-sheet peak for 1 wt% C_{16}-KTTKS solutions containing up to and including 0.7 wt% SDS. A feature at 1560 cm^{-1} is assigned to N-H bending vibrations and does not show trends as a function of [SDS] or temperature. At higher [SDS], the β-sheet peak disappears indicating the eventual SDS-induced breakup of the β-sheets. Concerning temperature dependence, the amide I' region spectra were essentially independent of temperature for 1% PA solutions containing up to 0.3 wt% SDS. At higher [SDS], the 1608 cm^{-1} β-sheet peak was found to reduce in intensity relative to the 1651 cm^{-1} disordered conformation peak (Fig.7b) pointing to thermally-induced disruption of the β-sheet secondary structure. These trends are

associated with the reduction in the intensity of the 4 nm peak in the SAXS profiles, relative to the 5.2 nm bilayer spacing peak intensity.

Other regions of the FTIR spectra provided information on the lipid chain ordering (CH_2 stretch region 2850-2950 cm^{-1}). Spectra in this region did not show large changes (other than in absolute absorbance) with SDS concentration, and it is difficult to deconvolute the contribution from SDS and C_{16}-KTTKS alkyl chains, so further discussion is prohibited. In the range 1400-1500 cm^{-1}, the CH_2 / CH_3 scissoring bands[31-33] near 1468 cm^{-1} also gives information on hydrocarbon chain (Fig.7c). Little temperature dependence was observed, however there was a strong concentration dependence at a given temperature. The peak at 1418 cm^{-1} appears to be exclusively associated with C_{16}-KTTKS, as it is not observed for SDS. A peak in this position has been observed for other PAs.[10, 34] We assign this feature to the C-O stretch, specifically at the CH_3CO linkage.[35] It is observed for all mixtures of SDS and C_{16}-KTTKS up to 0.9 wt% SDS under which conditions separately resolved 1418 cm^{-1} and 1468 cm^{-1} peaks disappear (Fig.7c). It indicates that the arrangement of CH_2/CH_3 groups in the alkyl chain is not significantly affected by binding of SDS. SDS binding is therefore associated with the peptide headgroup alone.

The rheological properties of the mixtures were investigated. Fig.8 shows the results of selected temperature ramps (performed at a fixed frequency ω = 0.6 rad s^{-1}). The 1% solution of C_{16}-KTTKS with no added SDS forms a viscous solution, with a very low modulus (and $G'' > G'$). Upon addition of SDS, the modulus at a given frequency increases significantly up to 0.3 wt% SDS. The system under these

conditions forms a hydrogel, since G' is significantly larger than G" and both are nearly independent of frequency. SI Fig.4 shows the cloudy fluid appearance of the samples at low [SDS] (cloudiness is due to the formation of lengthy aggregate structures), a gel is formed at 0.3 wt% SDS. At higher [SDS] (eg 0.7 wt%) the samples become fluid again, and the cloudiness is reduced due to the breakup of the extended aggregate structures. The gel-fluid transition upon further increase of [SDS] was quantified by dynamic shear rheometry measurements. Frequency sweep data (not shown) reveals that the modulus decreases on increase of [SDS], sharply from $G' = 10^5$ Pa for 0.3% SDS to $G' < 10$ Pa for 0.4% SDS, both at a reference frequency $\omega = 10$ rads^{-1}, and hydrogel properties are lost. Temperature ramps were also performed to examine thermal phase transitions. These also reveal a pronounced phase transition occurring between 35 ^{o}C and 44 ^{o}C for the mixtures with 0.1% SDS or 0.2% SDS. There is a nearly two order of magnitude decrease in modulus for the mixture with 0.1 wt% SDS on increasing temperature over this interval (Fig.8). The fact that this transition occurs near body temperature (37 ^{o}C) may be of potential relevance to responsive systems based on these PAs for biomedical applications. The thermal transitions are correlated to the transitions observed by SAXS, and more particularly to the reduction in β-sheet content revealed by FTIR. In addition, the observation of a gel around 0.3 wt% SDS is related to the formation of a network of twisted fibrils with a highly extended conformation, i.e. large persistence length (Fig.2 and SI Fig.1).

Summary and Discussion

In summary, addition of SDS can be used to induce gelation in solutions of the collagen-stimulating PA C_{16}-KTTKS. This may be very useful in applications in personal care products for slow release applications. The thermal melting transition at around body temperature is also highly relevant to such applications. A detailed physico-chemical study using AFM, TEM, STEM and SAXS, of the self-assembly of mixtures of C_{16}-KTTKS and SDS has revealed transitions in morphology upon addition of SDS from flat tapes for C_{16}-KTTKS through twisted ribbons to fibrillar structures. This is shown schematically in Fig.9. Electrophoretic mobility experiments reveal that this transition is not solely related to electrostatic phenomena since aggregates with different morphologies are observed for equal but opposite charge densities. The system is complex involving multiple equilibria between the ionic species present, but also hydrophobic interactions of the lipid chains, hydrogen bonding interactions within the peptide headgroup and chirality from the amino acid residues. Nevertheless, in a simplified picture the calculated net charge on the peptides is in reasonable agreement with the electrophoretic mobility measurements. SAXS also shows a fine balance between thermal energy and the other contributions to the total energy of the system. Further work is planned to investigate this in more detail.

Another remarkable finding from this work is the observation of longitudinal stripes within the aggregates. AFM and TEM reveal a 4 nm stripe spacing. The presence of striped aggregates increases with SDS concentration. Some striped tapes are observed at low [SDS], and a proposed model for these is sketched in Fig.9. We believe that the presence of longitudinal stripes, along with the coexistence of 4 nm and 5.2 nm bilayer spacings in the SAXS profiles can be explained using this model. It consists

of isolated sheets of bilayers stabilized by β-sheet H-bonding. The stacking distance of the β-sheets may be expanded due to electrostatic interactions between the condensed counterions and the lysine side chains on C_{16}-KTTKS, leading to an expanded spacing of the sheets relative to a conventional β-sheet structure, for which the usual spacing is around 1-1.2 nm. In reality, the system probably at low [SDS] only contains a small fraction of striped tapes, the majority are unstriped and consist of PA bilayers with a "standard" β-sheet packing arrangement, i.e. 1-1.2 nm stacking distance of sheets and 0.47 nm strand spacing within the sheets.[11] As noted above, the SAXS (Fig.5) and XRD data (Table 1) indicate the development of the expanded 4 nm spacing with increasing [SDS] (also XRD shows a small but significant change in the packing of the strands when the stripes form). In addition, SAXS shows a sensitive thermal dependence, increasing temperature leads to a loss of the 4 nm stripe periodicity and an enhancement of the 5.2 nm bilayer spacing. Upon increasing SDS concentration striped twisted ribbons and subsequently, at higher [SDS], fibrils are observed.

A possible explanation of the stripe pattern on the tapes in terms of SDS condensation on the surface of the aggregates has been excluded, since a small proportion of striped tapes are actually observed in water, in the absence of SDS. In addition, stripes are observed for the related PA C_{16}-ETTES in the absence of SDS.[36] The formation of stripes due to SDS condensation in the presence of divalent cations, that leads to the formation of stripes with a 5 nm spacing, has been revealed by AFM imaging on graphite.[37] It is possible that this does play a role in the development of stripes on the fibrillar aggregates at high [SDS]. In their study on C_{16}-OVEVE, Stupp and coworkers observed stripe formation upon increasing pH with sodium hydroxide. [10]

The situation here is more complex as the addition of SDS causes morphology transitions, in addition to stripe formation. The calculated degrees of dissociation of the carboxyl termini suggest that C_{16}-KTTKS behaves essentially as a divalent cationic macroion. Divalent cations are known to have remarkable properties in polyelectrolyte solutions and other self-assembling systems.[38-42] In addition, Manning condensation[43, 44] is well documented for polyelectrolyte solutions such as DNA or poly(styrene sulfonate).[38, 39, 41] The presence of condensed counterions in the present system, can in fact be justified by applying the Manning condensation threshold criterion to the self-assembled C_{16}-KTTKS structure. Indeed, by considering the self-assembly of C_{16}-KTTKS in the absence of SDS, which bears an average net charge of +2e per molecule, and remembering that two contiguous Matrixyl molecules along the fibril long axis are separated by a distance L=0.47 nm (the β-sheet spacing) the number charge linear density ρ for a single strand of PA would be approximately $\rho = +2/L \approx +4.3$ nm^{-1}. Catastrophic counterion condensation starts when the Oosawa–Manning parameter, expressed as ρl_B where l_B is the Bjerrum length, reaches values larger than 1. By taking l_B equal to 0.7 nm for water, ρl_B is calculated to be of the order of 3, which infers then the presence of condensed counterions. Furthermore, counterion condensation, predicted here to occur for the neat Matrixyl only, is likely to occur also in the presence of extra salt (e.g. SDS in the present case), as recently theoretically demonstrated in systems containing salt.[40] This argument, together with the closely matching periodicity of SDS bilayers and the stripes, suggests that SDS could also take an important role in the formation of the observed stripes.

These morphological studies shed light on the rheological properties, especially the formation of a gel at an SDS concentration of 0.3 wt% (with 1 wt% C_{16}-KTTKS).

This is associated with the formation of a network of highly extended twisted fibrils. The thermal phase transitions revealed by temperature ramp experiments seem to be correlated to the loss of β-sheet structure on heating, as revealed by FTIR. This also leads to the loss of the 4 nm stripe periodicity in the SAXS patterns. At high SDS concentrations there is a re-entrant gel-sol transition which we ascribe to electrostatic repulsion effects (between SDS-decorated fibrils and/or involving counterion condensation, i.e. Manning condensation).

Our work reveals that addition of SDS can be used to control the morphology of PA self-assemblies, which in turn can be used to tune rheological properties with considerable scope to create novel bionanomaterials for important applications in skincare and tissue engineering more broadly. Further work is underway to pursue these applications, and to study the relationship between self-assembly and bioactivity.

Acknowledgements. This work was supported by EPSRC grants EP/F048114/1 and EP/G026203/1 to IWH. Beamtime at the ESRF was awarded under reference SC-2985. X-ray diffraction experiments were performed in the BioCentre at the University of Reading. Dr Rebecca Green is acknowledged for access to the FTIR instrument.

References

[1] G. A. Silva, C. Czeisler, K. L. Niece, E. Beniash, D. A. Harrington, J. A. Kessler, and S. I. Stupp, *Science*, 2004, **303**, 1352.

[2] V. M. Tysseling-Mattiace, V. Sahni, K. L. Niece, D. Birch, C. Czeisler, M. G. Fehlings, S. I. Stupp, and J. A. Kessler, *J. Neurosci.*, 2008, **28**, 3814.

[3] R. N. Shah, N. A. Shah, M. M. D. Lim, C. Hsieh, G. Nuber, and S. I. Stupp, *Proc. Natl. Acad. Sci. U. S. A.*, 2009, **107**, 3293.

[4] C. W. Bond, N. L. Angeloni, D. A. Harrington, S. I. Stupp, K. E. McKenna, and C. A. Podlasek, *J. Sex. Med.*, 2011, **8**, 78.

[5] F. Versluis, H. R. Marsden, and A. Kros, *Chem. Soc. Rev.*, 2010, **39**, 3434.

[6] D. W. P. M. Löwik and J. C. M. van Hest, *Chem. Soc. Rev.*, 2004, **33**, 234.

[7] S. Cavalli and A. Kros, *Adv. Mater.*, 2008, **20**, 627.

[8] H. G. Cui, M. J. Webber, and S. I. Stupp, *Peptide Science*, 2010, **94**, 1.

[9] I. W. Hamley *Soft Matter*, 2011, **7**, 4122.

[10] H. Cui, T. Muraoka, A. G. Cheetham, and S. I. Stupp, *Nano Letters*, 2009, **9**, 945.

[11] V. Castelletto, I. W. Hamley, J. Perez, L. Abezgauz, and D. Danino, *Chem. Comm.*, 2010, **46**, 9185.

[12] K. Katayama, J. Armendarizborunda, R. Raghow, A. H. Kang, and J. M. Seyer, *J. Biol. Chem.*, 1993, **268**, 9941.

[13] K. L. Niece, J. D. Hartgerink, J. J. J. M. Donners, and S. I. Stupp, *J. Am. Chem. Soc.*, 2003, **125**, 7146.

[14] H. A. Behanna, J. Donners, A. C. Gordon, and S. I. Stupp, *J. Am. Chem. Soc.*, 2005, **127**, 1193.

[15] L. Aulisa, N. Forraz, C. McGuckin, and J. D. Hartgerink, *Acta Biomater.*, 2009, **5**, 842.

[16] J. S. Wall and J. F. Hainfeld, *Annual Review of Biophysics and Biophysical Chemistry*, 1986, **15**, 355.

[17] D. Thomas, P. Schultz, A. C. Steven, and J. S. Wall, *Biology of the Cell*, 1994, **80**, 181.

[18] O. S. Makin, P. Sikorski, and L. C. Serpell, *J. Appl. Cryst.*, 2007, **40**, 966.

[19] J. Adamcik, J. M. Jung, J. Flakowski, P. De Los Rios, G. Dietler, and R. Mezzenga, *Nature Nanotech*, 2010, **5**, 423.

[20] V. Castelletto, I. W. Hamley , C. Cenker, U. Olsson, J. Adamcik, R. Mezzenga, J. F. Miravet, B. Escuder, and F. Rodriguez-Llansola, *J. Phys. Chem. B*, 2011, **115**, 2107.

[21] J. Adamcik, V. Castelletto, I. W. Hamley , and R. Mezzenga, *Angew. Chem., Int. Ed. Engl.*, 2011, **50**, 5495.

[22] J. Adamcik and R. Mezzenga, *Soft Matter*, 2011, **7**, 5437.

[23] L. Alderighi, P. Gans, A. Ienco, D. Peters, A. Sabatini, and A. Vacca, *Coord. Chem. Rev.*, 1999, **184**, 311.

[24] S. Paula, W. Sus, J. Tuchtenhagen, and A. Blume, *J. Phys. Chem.*, 1995, **99**, 11742.

[25] D. F. Evans and H. Wennerström, 'The colloidal domain. Where physics, chemistry, biology and technology meet', Wiley, 1999.

[26] R. J. Hunter, 'Foundations of colloid science', Oxford University Press, 2001.

[27] M. Benrraou, B. L. Bales, and R. Zana, *J. Phys. Chem. B*, 2003, **107**, 13432.

[28] P. C. Griffiths, N. Hirst, A. Paul, S. M. King, R. K. Heenan, and R. Farley, *Langmuir*, 2004, **20**, 6904.

[29] V. Y. Bezzobotnov, S. Borbély, L. Cser, B. Faragó, I. A. Gladkih, Y. M. Ostanevich, and S. Vass, *J. Phys. Chem.*, 1988, **92**, 5738.

[30] M. Bergström and J. S. Pedersen, *J. Phys. Chem. B*, 1999, **103**, 8502.

[31] Y. P. Zhang, R. Lewis, R. S. Hodges, and R. N. McElhaney, *Biochemistry*, 1992, **31**, 11572.

[32] O. Reis, R. Winter, and T. W. Zerda, *Biochimica et Biophysica Acta - Biomembranes*, 1996, **1279**, 5.

[33] D. J. Moore, M. E. Rerek, and R. Mendelsohn, *J. Phys. Chem. B*, 1997, **101**, 8933.

[34] S. E. Paramonov, H.-W. Jun, and J. D. Hartgerink, *J. Am. Chem. Soc.*, 2006, **128**, 7291.

[35] L. J. Bellamy, 'The infra-red spectra of complex molecules', Chapman and Hall, 1975.

[36] I. W. Hamley , A. Dehsorkhi, and V. Castelletto, *Soft Matter*, 2011, submitted.

[37] E. J. Wanless and W. A. Ducker, *Langmuir*, 1997, **13**, 1463.

[38] B. L. Rivas and I. Moreno-Villoslada, *J. Phys. Chem. B*, 1998, **102**, 6994.

[39] L. Belloni, *Colloid Surf. A-Physicochem. Eng. Asp.*, 1998, **140**, 227.

[40] M. Deserno, C. Holm, and S. May, *Macromolecules*, 2000, **33**, 199.

[41] Y. B. Zhang, J. F. Douglas, B. D. Ermi, and E. J. Amis, *J. Chem. Phys.*, 2001, **114**, 3299.

[42] C. R. Safinya, U. Raviv, D. J. Needleman, A. Zidovska, M. C. Choi, M. A. Ojeda-Lopez, K. K. Ewert, Y. L. Li, H. P. Miller, J. Quispe, B. Carragher, C. S. Potter, M. W. Kim, S. C. Feinstein, and L. Wilson, *Adv. Mater.*, 2011, **23**, 2260.

[43] G. S. Manning, *Q. Rev. Biophys.*, 1978, **11**, 179.

[44] G. S. Manning, *Acc. Chem. Res.*, 1979, **12**, 443.

Tables

Table 1. XRD peak positions from patterns obtained from solutions of 1% C_{16}-KTTKS with the indicated amounts of added SDS. Here **a** denotes the bilayer spacing (52.5 Å) and **b** denotes the stripe spacing (40 Å). sho denotes a shoulder peak.

Sample / Peak	0% SDS	0.1% SDS	0.2% SDS	0.3% SDS	0.4% SDS	0.45% SDS	0.7% SDS	0.9% SDS
Long spacing **a** 1st order								
Long spacing **b** 1st order							40.8	
Long spacing **a** 2nd order	26.4	26.1	26.1	27.9 (sho)				
Long spacing **b** 2nd order				20.2 (sho)	21.0	20.5	19.8	19.9
16-17 Å spacing		17.4 (sho, 3rd order of **a**)	17.3 (sho, 3rd order of **a**)		16.8 (3rd order of **a**)			
13-14 Å spacing	13.92	12.83 (4th order of **a**)	12.81 (4th order of **a**)	13.98 (3rd order of **b**)	14.0 (3rd order of **b**)	13.8 (3rd order of **b**)	13.2 (3rd order of **b**)	13.2 (3rd order of **b**)
11 Å spacing (β-sheet stacking distance)	11.3	11.5	11.5					
7-9 Å spacing	9.1/7.7/ 6.7/6.5	9.1/6.7	9.1/6.7	8.8/7.9		8.3 / 7.65		9.7
β-strand spacing	4.78	4.82	4.81	4.67	4.71	4.68	4.73	4.71

Figures

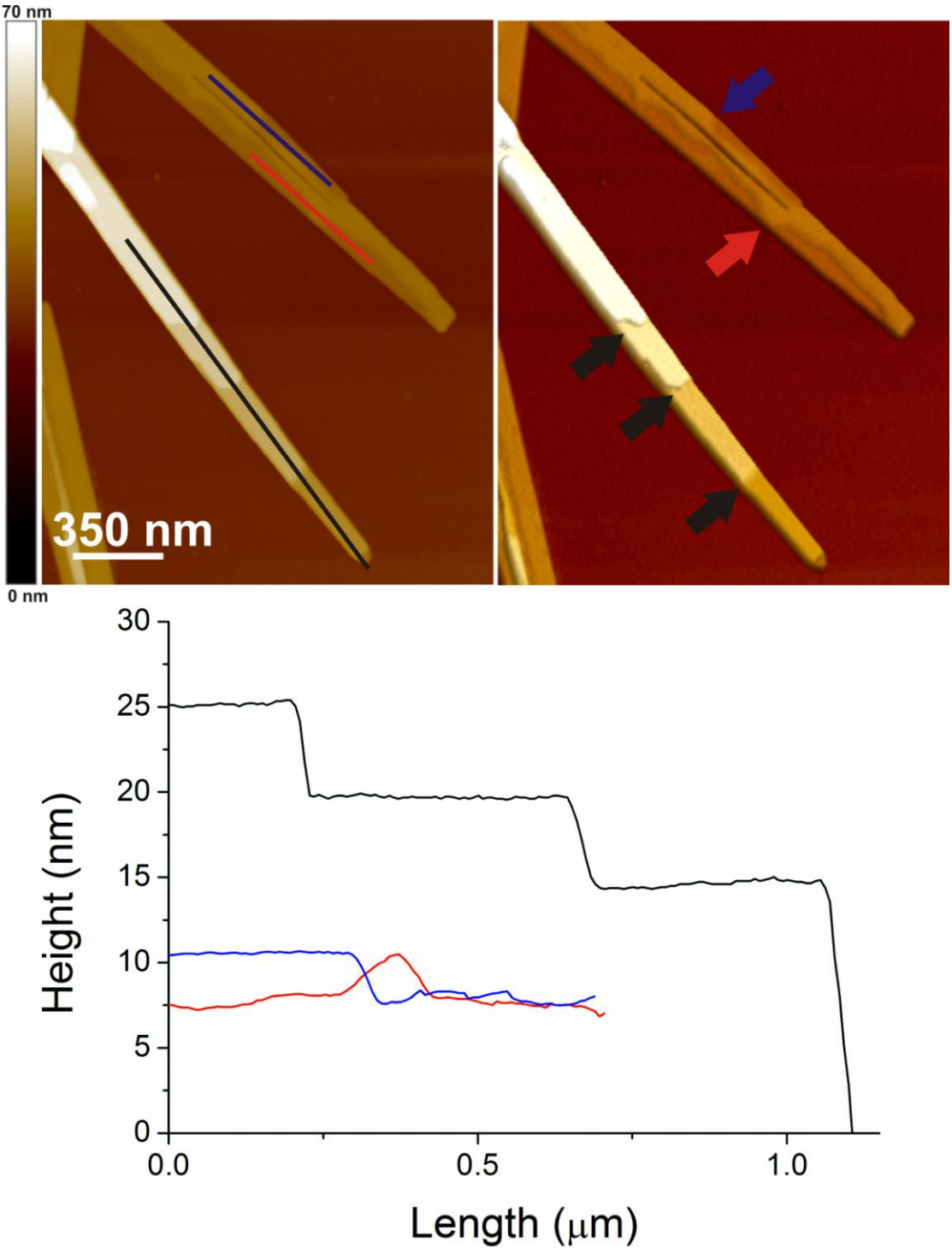

Figure 1. AFM images (left upper part) and corresponding 3D image (right upper part) of 1 wt% of C_{16}-KTTKS deposited on mica. Lower part represents the longitudinal height profiles of tapes. One step on black curve is about 5.3 nm. The step on the blue and red curve is about 2.65 nm.

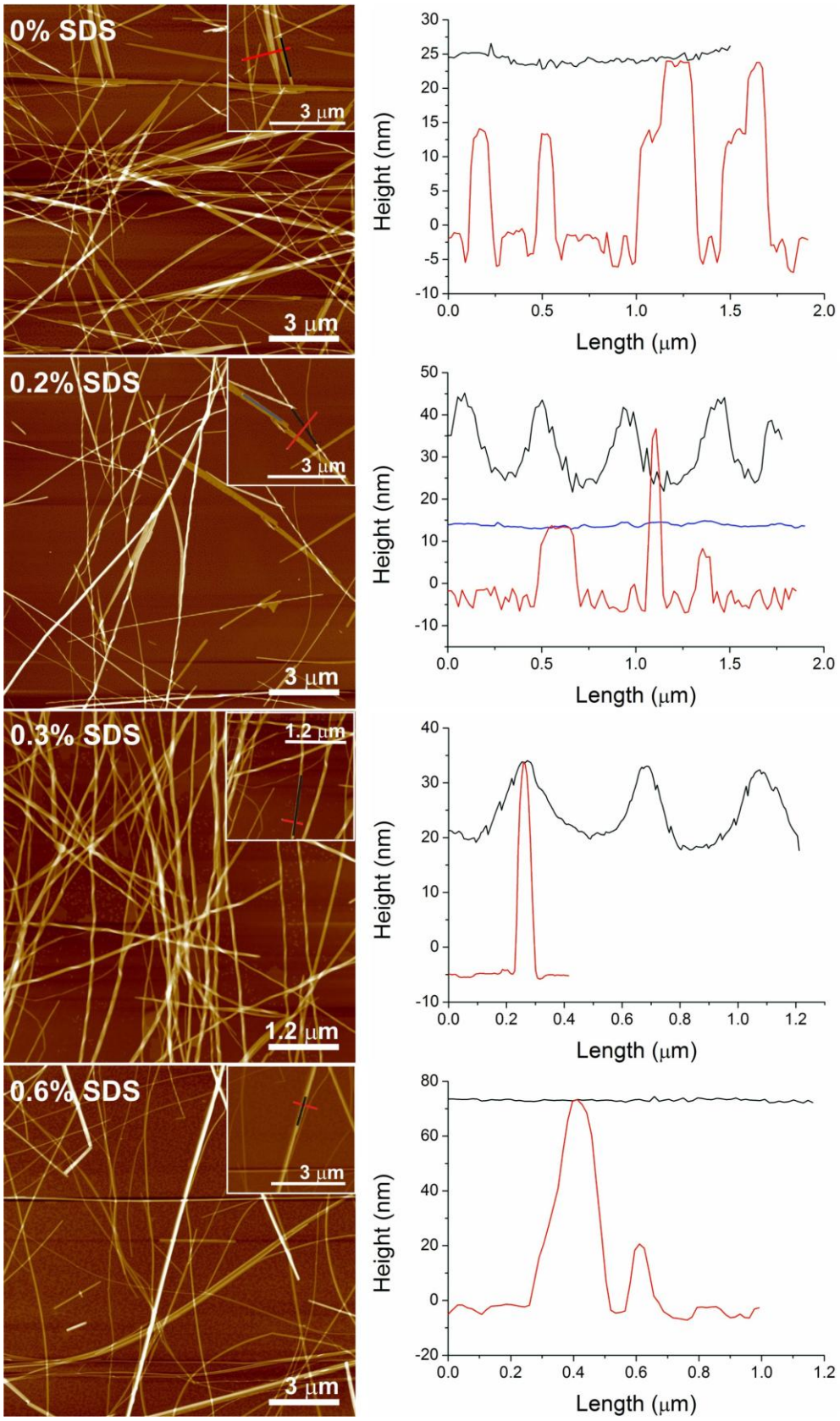

Figure 2. AFM images of C_{16}-KTTKS with different SDS concentrations and their corresponding transversal (red curve) and longitudinal (black and blue curve) height profiles. The insets show the objects selected for the height profile analysis.

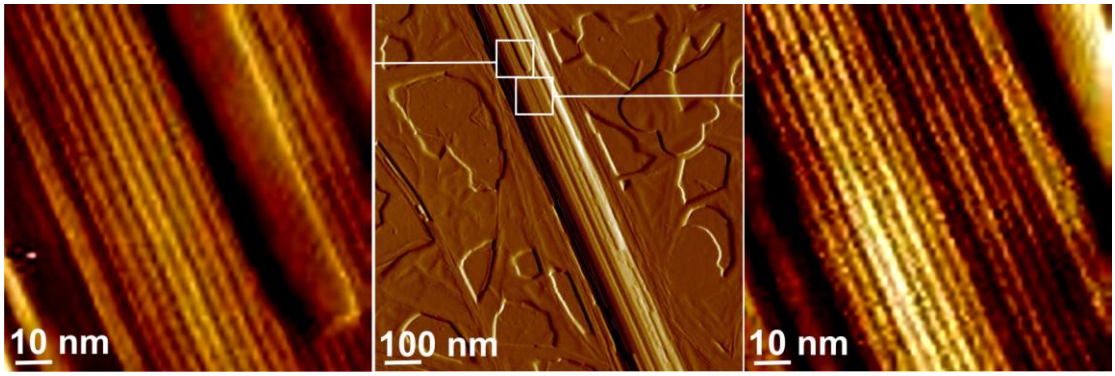

Figure 3. AFM amplitude images of a cylindrical aggregate formed by C_{16}-KTTKS with 0.9 wt% added SDS. Upper and lower parts show high resolution images of surfaces with the presence of stripes with a periodicity about 4.2 nm.

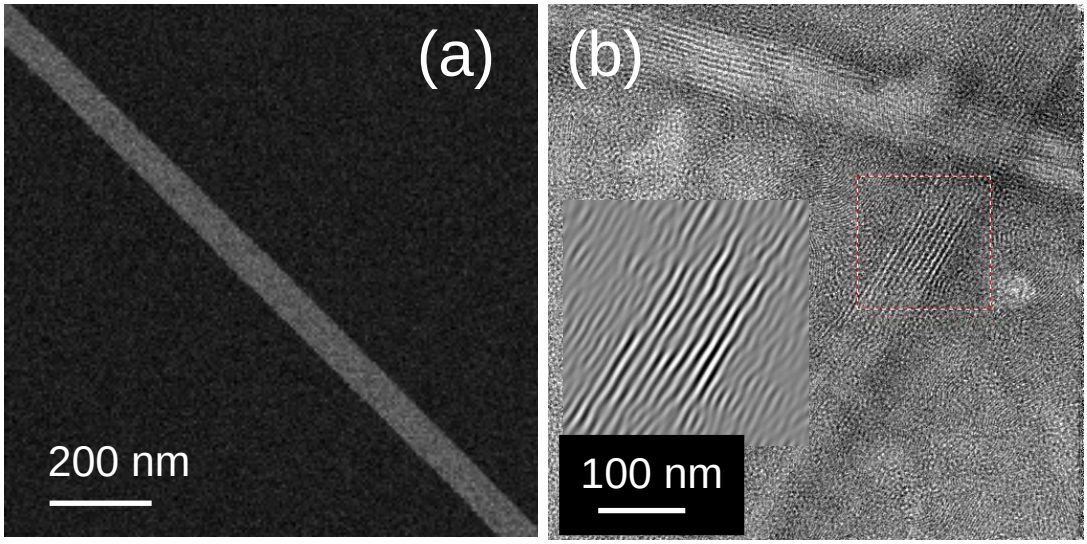

Figure 4. Electron microscopy images of tapes of C_{16}-KTTKS. (a) STEM image from a 3 wt% sample (0 wt% SDS), (b) Negative stain TEM image from a 1 wt% sample with 0.1 wt% SDS added (inset-Fourier filtered image of region highlighted).

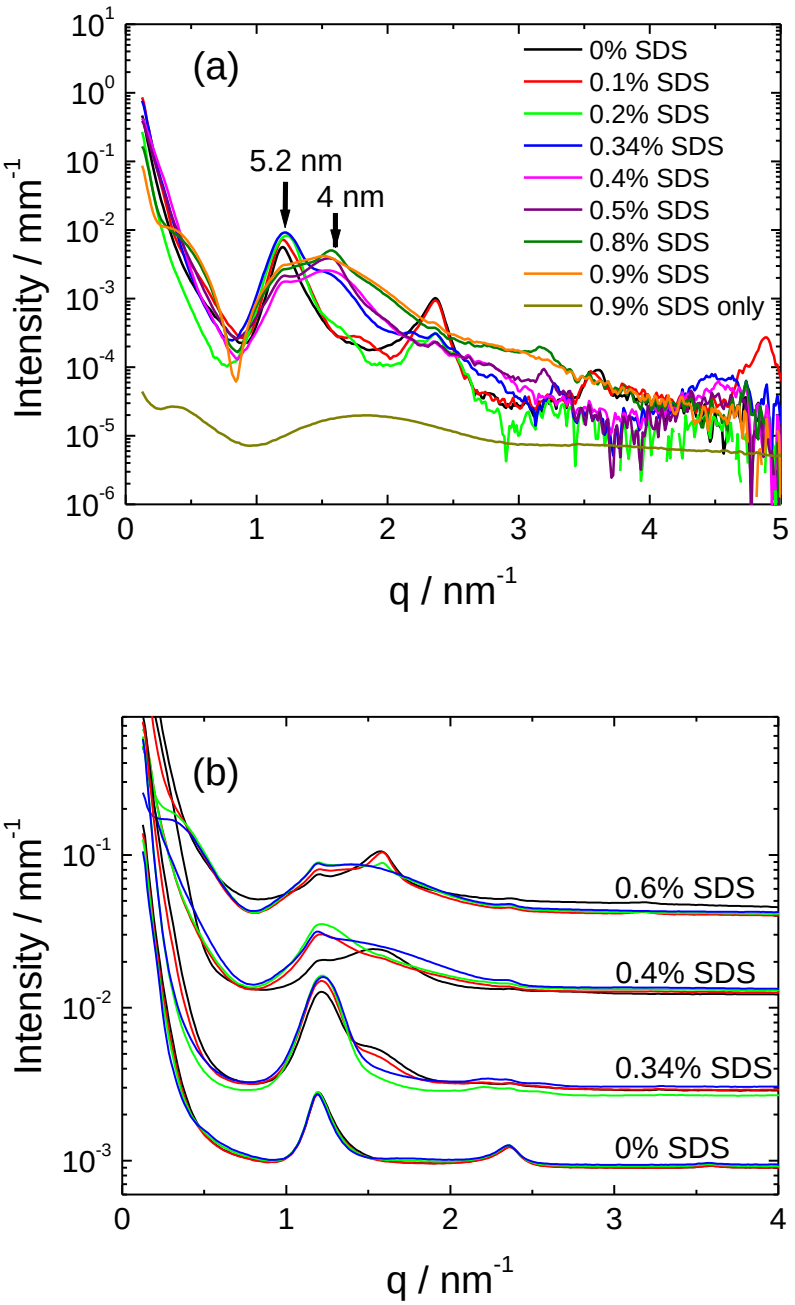

Figure 5. SAXS data. (a) Profiles as a function of SDS concentration (at 25 ^{o}C) for 1 wt% C_{16}-KTTKS samples at the SDS concentrations indicated, (and for comparison, the data for 0.9 wt% SDS). (b) SAXS data for 1 wt% C_{16}-KTTKS with (and without) added SDS as a function of temperature (selected every 10 ^{o}C – black lines 25 ^{o}C, red lines 35 ^{o}C, green lines 45 ^{o}C, blue lines 55 ^{o}C). The curves are presented for convenience without background subtraction and are displaced vertically to aid presentation.

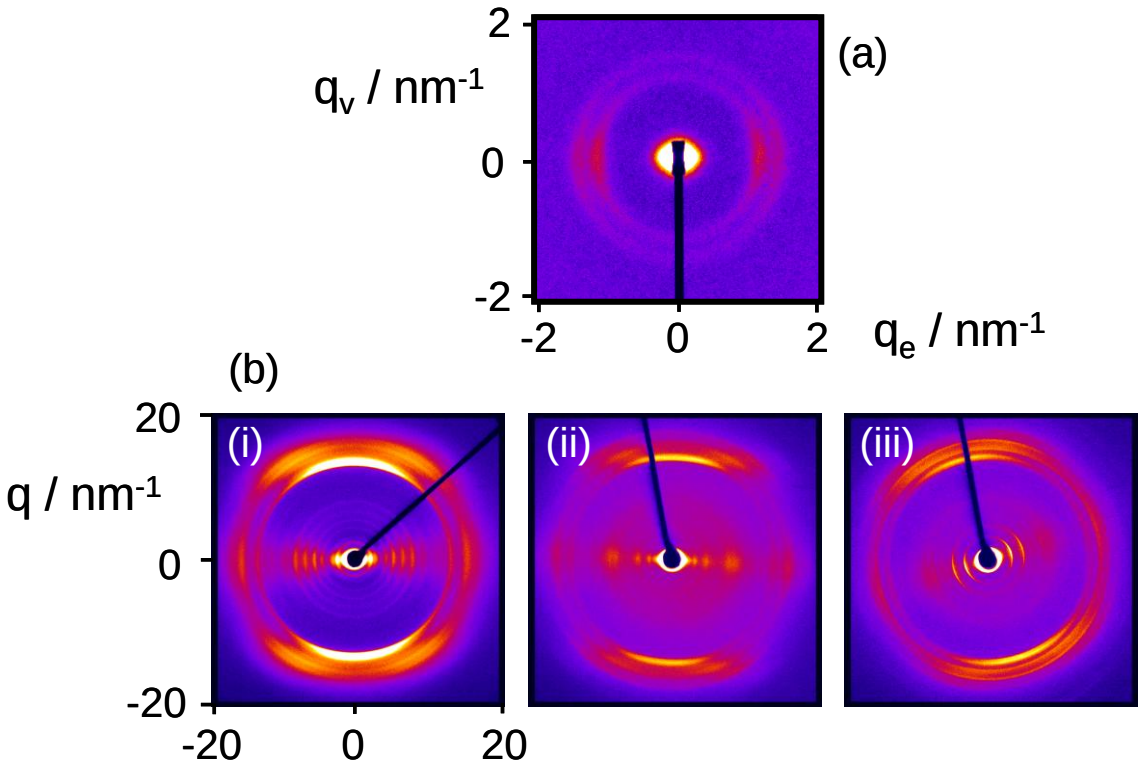

Figure 6. Two-dimensional X-ray scattering data. (a) Two-dimensional SAXS pattern for a shear aligned sample of 1 wt% C_{16}-KTTKS + 0.3 wt% SDS, the pattern is rotated through 90^o (flow direction **v** vertical, **e** denotes vorticity direction) for comparison with fibre XRD images. (b) Selected fibre XRD patterns (approximately vertical fibre axis) for 1 wt% C_{16}-KTTKS plus (i) 0 wt% SDS, (ii) 0.5 wt% SDS, (iii) 0.9 wt% SDS.

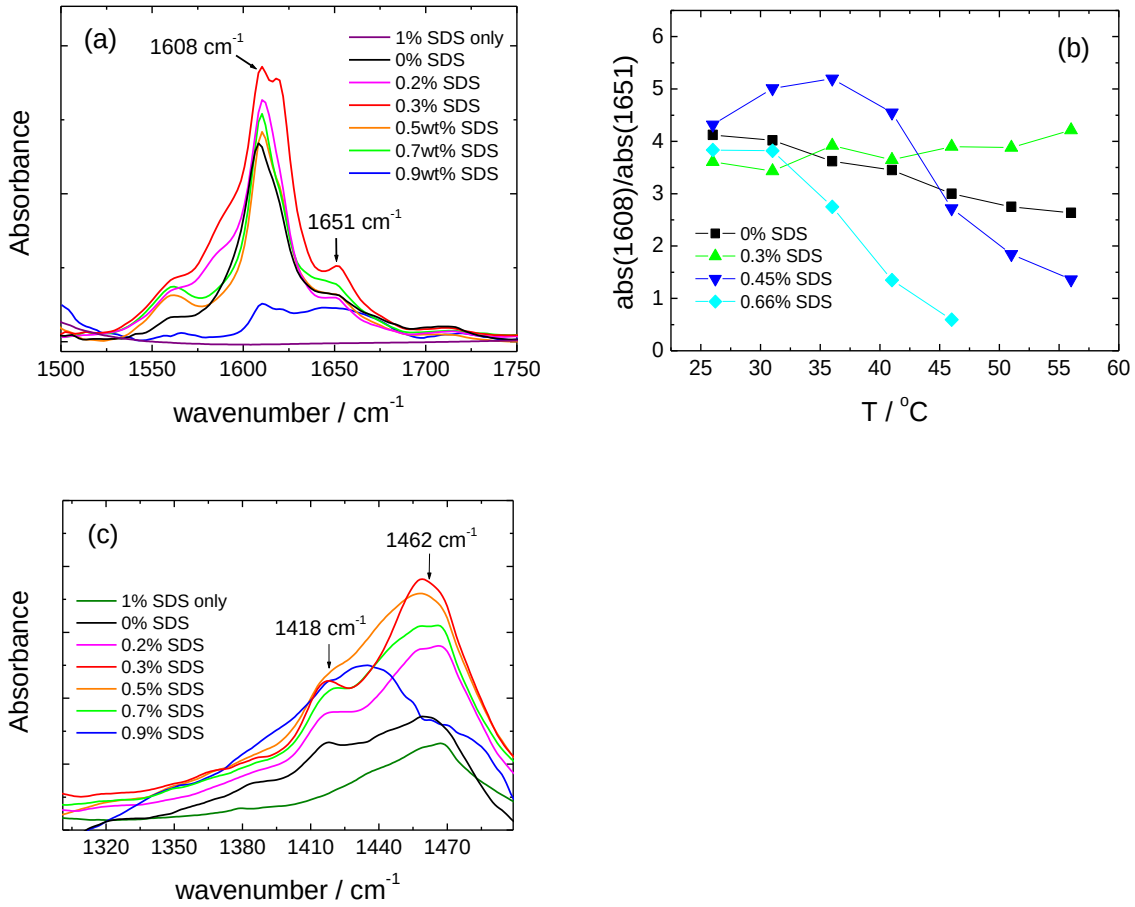

Figure 7. FTIR spectra from samples containing 1 wt % C_{16}-KTTKS with 0.1-0.9 wt% SDS at 25 °C. (a) Spectra in the amide I' region, (b) Temperature dependence of main amide I' peak intensity for selected SDS concentrations, (c) Spectra in the region of the CH_2/CH_3 scissoring bands.

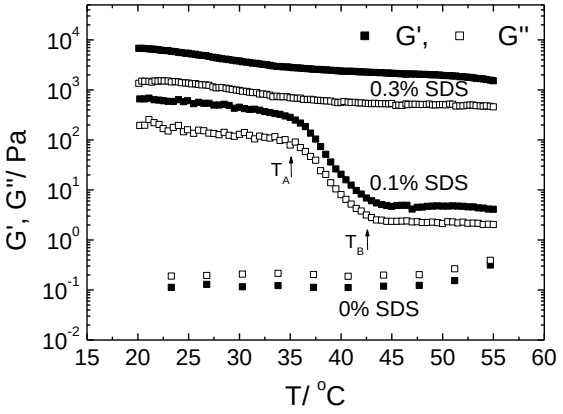

Figure 8. Rheology data for 1 wt% C_{16}-KTTKS solutions. Temperature ramps performed at 6 rad s^{-1} except 0% SDS at 0.2 rad s^{-1}, controlled strain < 0.1 Pa of dynamic shear moduli for selected concentrations.

.

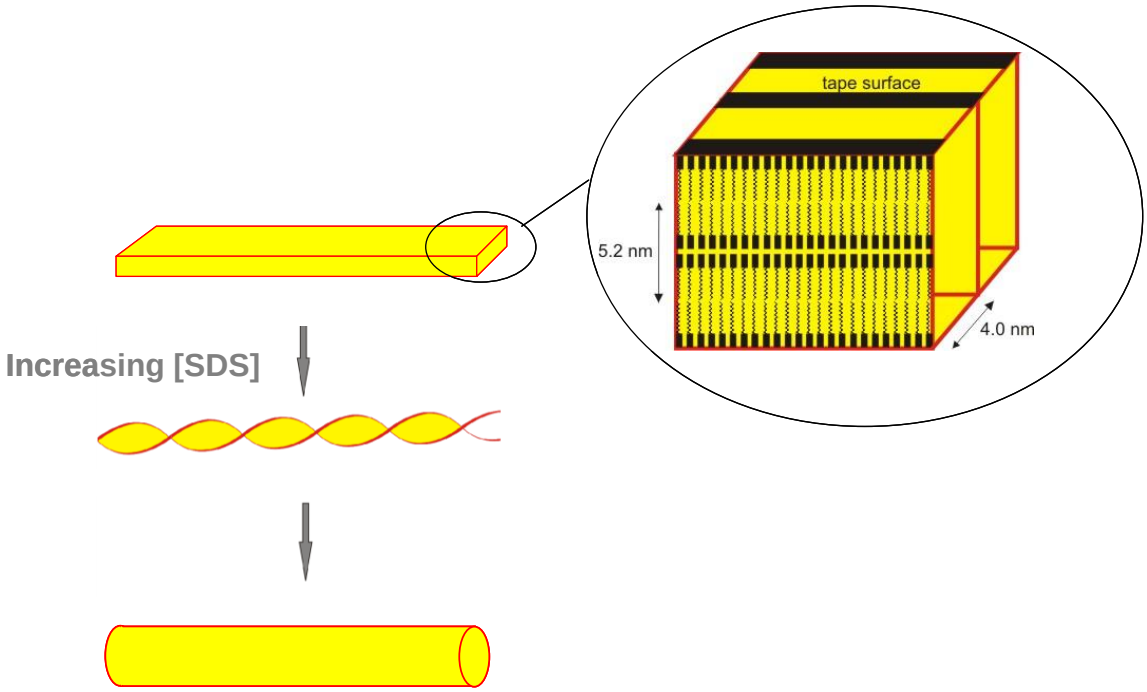

Figure 9. Left: Schematic of observed morphology transitions. Right inset: Proposed model for striped tapes – similar structural periodicities will give rise to the striped twisted and straight fibrillar structures on increasing SDS concentration.

TOC Entry